HHS Public Access

Author manuscript

Nucl Med Biol. Author manuscript; available in PMC 2016 November 01.

Published in final edited form as:

Nucl Med Biol. 2015 November ; 42(11): 816–823. doi:10.1016/j.nucmedbio.2015.07.010.

Evaluation of DOTA-chelated neurotensin analogs with spacer-enhanced biological performance for neurotensin-receptor-1-positive tumor targeting

Yinnong Jia, **Wen Shi**, **Zhengyuan Zhou**, **Nilesh K. Wagh**, **Wei Fan**, **Susan K. Brusnahan**, and **Jered C. Garrison***

Department of Pharmaceutical Sciences, University of Nebraska Medical Center, 985830, Nebraska Medical Center, Omaha, NE, USA 68198-5830

Abstract

Introduction—Neurotensin receptor 1 (NTR1) is overexpressed in many cancers types. Neurotensin (NT), a 13 amino acid peptide, is the native ligand for NTR1 and exhibits high (nM) affinity to the receptor. Many laboratories have been investigating the development of diagnostic and therapeutic radiopharmaceuticals for NTR1-positive cancers based on the NT peptide. To improve the biological performance for targeting NTR1, we proposed NT analogs with 1,4,7,10-tetraazacyclododecane-1,4,7,10-tetraacetic acid (DOTA) chelation system and different lengths of spacers.

Methods—We synthesized four NTR1-targeted conjugates with spacer lengths from 0 to 9 atoms (null (N0), β-Ala-OH (N1), 5-Ava-OH (N2), and 8-Aoc-OH (N3)) between the DOTA and the pharmacophore. *In vitro* competitive binding, internalization and efflux studies were performed on all four NT analogs. Based on these findings, metabolism studies were carried out on our best performing conjugate, ^{177}Lu-N1. Lastly, *in vivo* biodistribution and SPECT/CT imaging studies were performed using ^{177}Lu-N1 in an HT-29 xenograft mouse model.

Results—As shown in competitive binding assay, the NT analogs with different spacers (N1, N2 and N3) exhibited lower IC_{50} values than the NT analog without a spacer (N0). Furthermore, N1 revealed higher retention in HT-29 cells with more rapid internalization and slower efflux than the other NT analogs. *In vivo* biodistribution and SPECT/CT imaging studies of ^{177}Lu-N1 demonstrated excellent accumulation (3.1 ± 0.4 %ID/g) in the NTR1-positive tumors at 4 h post-administration.

Conclusions—The DOTA chelation system demonstrated some modest steric inhibition of the pharmacophore. However, the insertion of a 4-atom hydrocarbon spacer group restored optimal binding affinity of the analog. The *in vivo* assays indicated that ^{177}Lu-N1 could be used for imaging and radiotherapy of NTR1-positive tumors.

*Corresponding Author: Jered C. Garrison, PhD., Phone Number: 001-402-559-3453, Fax: 001-402-559-9365, jcgarrison@unmc.edu.

The authors have no potential conflict of interest relevant to this article.

Keywords

NT; NTR1; Lutetium-177; diagnostic imaging; HT-29; colon cancer

Introduction

The neurotensin receptor 1 (NTR1) is a G protein-coupled receptor of the neurotensin receptor family, of which there are three known members[1]. NTR1 has been shown to be up-regulated in numerous cancer types, including colon[2], breast[3], and pancreatic cancer[4]. The overexpression of NTR1 has been attributed to cancer cells as a crucial growth signaling pathway[5,6]. Studies have shown a strong link between NTR1 expression and the progression of many cancer types[2,5,7].

One area of NTR1 drug development being actively explored is NTR1-targeted diagnostic and therapeutic radiopharmaceuticals. The majority of these agents are based on neurotensin (NT), a 13-amino-acid peptide which exhibits nanomolar binding affinity to NTR1[8]. The C-terminus of NT is responsible for binding to NTR1, thus research has focused largely on employing NT(8–13) and NT(6–13) fragments in drug development[9]. One major obstacle that has hampered the development of NTR1-targeted radiopharmaceuticals is the rapid proteolytic degradation of the NT in serum. The main degradation sites are the Arg^{8}-Arg^{9}, Pro^{10}-Tyr^{11} and Try^{11}-Ile^{12} bonds in the NT structure[10]. To enhance the potential of NTR1-targeted radiopharmaceuticals, Schubiger, Garcia-Garayoa and others have reported promising strategies to metabolically stabilize the NTR1-targeted agents[11–13]. These modifications consist of replacing selected amino acids at the degradation sites with non-natural counterparts to inhibit proteolytic cleavage. Among these stabilizing modifications, replacement of a secondary amide with a tertiary amide (N-CH_3) at the Arg^{8} position, replacement of Tyr^{11} with 2,6-dimethyl tyrosine (Dmt), and replacement of Ile^{12} with *tert*-leucine (Tle), have been shown to substantially inhibit degradation and improve *in vivo* stability [11,14,15].

A principal chelator used in the design of radiometal-based theranostic agents is 1,4,7,10-tetraazacyclododecane-1,4,7,10-tetraacetic acid (DOTA) [14]. The primary reason for the extensive utilization of this macrocycle is its inherent *in vivo* stability with a variety of clinically relevant radiometals. The incorporation of DOTA on the N-terminus of the pharmacophore has been accomplished with diverse receptor-avid peptides[16]. However, for some peptides, placement of the DOTA chelation system too close to the pharmacophore can sterically interfere with the binding of the agent to the receptor of interest[17]. In this circumstance, inclusion of a linking group to increase the distance between DOTA and the pharmacophore can restore optimal binding[18,19].

In this study, we investigated the extent to which distance between the DOTA chelation system and a NT(6–13) peptide fragment affects binding affinity. The NT(6–13) analog ([N-α-Me^{8},Dmt^{11},Tle^{12}]NT(6–13)) chosen for this study includes all three of the stabilizing modifications listed above. Hydrocarbon linking groups of various lengths (0 – 9 atoms) were incorporated between the DOTA chelation system and the N-terminus of the NT pharmacophore. Once in hand, the *in vitro* binding and cellular uptake properties of the

NTR1-targeted conjugates were investigated in the NTR1-positive HT-29 human colon cancer cell line. Based on these results, we report the preliminary biodistribution and SPECT/CT studies of our most promising radioconjugate.

Materials

Acetonitrile, formic acid, *N*,*N*-diisopropylethylamine (DIEA), *N*,*N*-dimethylformamide (DMF), dichloromethane (DCM), *N*,*N*'-dicyclohexylcarbodiimide (DCC) , *N*-methylpyrrolidone (NMP), 4-(2-hydroxyethyl)-1-piperazineethanesulfonic acid (HEPES), bovine serum albumin (BSA) and sodium dodecyl sulfate (SDS) were purchased from Fisher Scientific (Fair Lawn, NJ). Fluorenylmethyloxycarbonnyl (Fmoc)-protected natural amino acids, Fmoc-β-Ala-OH, Fmoc-Leu-Wang resin (100–200 mesh), and (1-Cyano-2-ethoxy-2-oxoethylidenaminooxy) dimethylamino-morpholino-carbenium hexafluorophosphate (COMU), were purchased from NovaBiochem (Hoherbrunn, Germany). Fmoc-N-Me-Arg(Pbf)-OH was produced by ChemPep, Inc. (Wellington, FL). Fmoc-2,6-dimethyl-L-tyrosine (Dmt) was from Ontario Chemicals, Inc (Guelph, ON, Canada). Fmoc-Tle-OH, Fmoc-8-Aoc-OH, and Fmoc-5-Ava-OH were purchased from CreoSalus (Louisville, KY). Lutetium-177 chloride ($^{177}LuCl_3$) was obtained from Perkin Elmer (Waltham, MA) with a specific activity of 32.3 Ci/mg. Naturally abundant lutetium chloride ($^{nat}LuCl_3$), triisopropylsilane and 3,6-dioxa-1,8-octanedithiol were from Sigma-Aldrich (St Louis, MO). Neurotensin (NT) was purchased from American Peptide, Inc. (Sunnyvale, CA). McCoy's 5A medium (1X; Iwakata & Grace Mod.) with L-glutamine was obtained from Mediatech, Inc. (Manassas, VA). TrypLE™ Express was purchased from Invitrogen (Grand Island, NY).

Methods

Cell culture

The human colon cancer cell line HT-29 was obtained from American Type Culture Collection (U.S.) and cultured under vendor-recommended conditions. Cells were passaged twice weekly in McCoy's 5A medium supplemented with 10% FCS, 100 IU/ml penicillin and 100 μg/ml streptomycin at 37 °C in a humidified incubator containing 5% CO_2.

Xenograft Models

All animal experiments were conducted in accordance with the Principles of Animal Care outlined by the National Institutes of Health and approved by the Institutional Animal Care and Use Committee of the University of Nebraska Medical Center. Eight-week-old Institute of Cancer Research severely combined immunodeficient (ICR SCID) mice were obtained from Charles River Laboratories (Wilmington, MA). Animals were housed five per cage in a light-and temperature-controlled environment. Food and water were given ad libitum. Bilateral HT-29 tumors were induced by subcutaneous injection of 4.0×10^6 cells in Matrigel (BD Biosciences). The tumors were allowed to grow for 2–3 weeks reaching maximal 1 cm in diameter before the mice were utilized in pharmacokinetic studies.

Solid-Phase Peptide Synthesis (SPPS)

Peptides were synthesized on an automated solid-phase Liberty microwave peptide synthesizer from CEM (Matthews, NC), employing traditional Fmoc chemistry. Briefly, the Fmoc-Leu-Wang resin (100 μmol of the resin-substituted peptide anchors) was deprotected by piperidine, resulting in the formation of a primary amine from which the C-terminus of the growing peptide was anchored. Fmoc-protected amino acids (300 μmol) were activated with COMU and sequentially conjugated to the resin. The resulting peptide was orthogonally deprotected and cleaved from the resin by shaking in a cocktail consisting of triisopropylsilane (0.125 ml), water (0.125 ml), 3,6-dioxa-1,8-octanedithiol (0.125 ml), and trifluoroacetic acid (4.625 ml) for 3 hours. The cleaved peptide was subsequently precipitated and washed thrice using cold (0 °C) methyl-*tert*-butyl ether (40 ml×3). The crude conjugate was dried by a CentriVap concentrator and weighed.

HPLC Purification and Analysis Methodology

HPLC/MS analyses were performed on a Waters (Milford, MA) e2695 system equipped with a Waters 2489 absorption detector and a Waters Q-Tof Micro electrospray ionization mass spectrometer. Sample purification for *in vitro* studies was performed on a Phenomenex (Torrance, CA) Jupiter 10 μm Proteo 250 × 4.6 mm C12 column with a flow rate of 1.5 mL/min. For bulk sample purification, a Phenomenex Jupiter 10 μm Proteo 250 × 10 mm C12 column was used with a flow rate of 5.0 mL/min. HPLC solvents consisted of H_2O containing 0.1% formic acid (solvent A) and acetonitrile containing 0.1% formic acid (solvent B). For unlabeled and $^{177/nat}$Lu-conjugates of N0 and N1, an initial gradient of 95% A: 5% B linearly decreased to 85% A: 15% B over a 15-minute time period. For unlabeled and $^{177/nat}$Lu-conjugates of N2, an initial gradient of 92% A: 8% B linearly decreased to 87% A: 13% B over a 15-minute time period. For unlabeled and $^{177/nat}$Lu-conjugates of N3, an initial gradient of 90% A: 10% B linearly decreased to 85% A: 15% B over a 15-minute time period. At the end of the run time for all HPLC experiments, the column was flushed with the gradient 5% A: 95% B and re-equilibrated to the starting gradient.

Labeling with $^{nat}LuCl_3$

Naturally abundant ^{nat}Lu was used to substitute for ^{177}Lu in the ES-MS and *in vitro* binding studies. A sample of conjugates (0.10 mg, 0.06 μmol) was dissolved in ammonium acetate buffer (0.5 M, 200 μL, pH 5.5) and mixed with a solution of $^{nat}LuCl_3$ (1.7mg, 6 μmol). The solution was heated for 60 min at 90 °C. After cooling to room temperature, ^{nat}Lu-conjugates were then peak purified by RP-HPLC in the same conditions above. All ^{nat}Lu-conjugates were ≥ 95% pure before mass spectrometric characterization and *in vitro* binding studies were performed.

Radiolabeling with $^{177}LuCl_3$

A sample of the conjugates (50 μg, 30 nmol)) was dissolved in ammonium acetate buffer (0.5 M, 100 μL, pH 5.5). $^{177}LuCl_3$ (37 MBq, 1 mCi, 0.18 nmol) was added to the vial containing the conjugate, and the solution was heated for 60 min at 90 °C. To separate radiolabeled peptides from unlabeled peptides on HPLC, 4–5 mg $CoCl_2$ were then added and incubated for 5 min at 90 °C to increase the hydrophobicity of unlabeled conjugates[20].

After cooling to room temperature, evaluation and purification of radiolabeled conjugate were performed on a Waters 1525 binary pump equipped with a Waters 2489 absorption detector and a Bioscan (Poway, CA) Flow Count radiometric detector system. The collected radioconjugate was concentrated with an Empore (Eagan, MN) C18 high performance extraction disk followed by elution with ethanol/sterile saline solution (6:4, 400 μL) to provide the radiolabeled conjugates in high purity.

Distribution coefficient

The distribution coefficient was determined (n = 6, 2 technical (tech) and 3 biological (bio) repeats) for each ^{177}Lu-labeled conjugate. In a 1.5 ml centrifuge tube, 0.5 mL of 1-octanol was added to 0.5 mL phosphate-buffered saline (pH 7.4) containing the radiolabeled peptide (500,000 cpm). The solution was vigorously stirred for 2 min at room temperature and subsequently centrifuged (8000 × *g*, 5 min) to yield two immiscible layers. Aliquots of 100 μL were taken from each layer and the radioactivity of each was quantified by an LTI (Elburn, IL) Multi-Wiper nuclear medicine gamma counter.

Receptor saturation

Receptor saturation studies were performed (n = 6, 2 tech and 3 bio repeats) using ^{177}Lu-N1 on the human colon cell line HT-29. HT-29 cells (1×10^6) were suspended in 1.5 ml low retention centrifuge tubes with 100 μl McCoy's medium (pH 7.4, 4.8 mg/mL HEPES, and 2 mg/mL BSA). ^{177}Lu-N1 (200,000 cpm, 100 μl) and a series of 100 μl N1 concentrations ranging from 0.469 nM to 120 nM were added for 45 min at 4 °C. Non-specific binding was determined using 3 μM N1 in the presence of the radioligand. The specific activity was determined as total binding activity minus non-specific binding. At the end of the incubation time, cells were aspirated and washed five times with cold medium and the remaining radioactivity was measured by gamma counter. Non-linear regression analysis was then performed using GraphPad Prism 5 (U.S.) to determine the B_{max} and K_d values for each experiment.

In vitro competitive binding studies

For *in vitro* binding studies, the half maximal inhibitory concentration (IC_{50}) for each conjugate was determined (n = 6, 2 tech and 3 bio repeats) for each ^{177}Lu-labeled conjugate using the human colon cancer cell line, HT-29. In these studies, ^{177}Lu-N1 served as the control and as the radioligand for comparing the relative effectiveness of the conjugates (N0–3 and NT). Briefly, HT-29 cells (~1×10^6) were suspended in 100 μl McCoy's medium (pH 7.4, 4.8 mg/mL HEPES, and 2 mg/mL BSA) and incubated at 37 °C for 45 min in the presence of radiolabeled ^{177}Lu-N1 (100,000 cpm, 100 μl) and various concentrations of the unlabeled conjugates and ^{nat}Lu-conjugates (100 μl). At the end of the incubation, the cells were centrifuged, aspirated and washed with media five times. The cell-associated radioactivity was measured using a gamma counter and the IC_{50} values determined by nonlinear regression using the one-binding site model of GraphPad Prism 5 (U.S.).

In vitro internalization and efflux studies

Internalization studies were performed (n = 6, 2 tech and 3 bio repeats) for each ^{177}Lu-labeled conjugate using HT-29 cells in 1.5-ml centrifuge tubes. HT-29 cells (~1×10^6) were suspended in 100 μl McCoy's media (pH 7.4, 4.8 mg/mL HEPES, and 2 mg/mL BSA). Cells were incubated for various times up to 2 h at 37°C in the presence of 100,000 cpm of each ^{177}Lu-radioconjugates. During the incubation, at time points 15, 30, 60 and 120 min, cells were washed five times with media to remove the unbound peptide. Surface-bound radioactivity was removed by washing the cells twice with an acidic buffer (50 mM glycine-HCl/0.1 M NaCl buffer, pH 2.8). The amount of radioactivity in each cellular pellet was measured as the internalized fraction by gamma counter.

For efflux studies, HT-29 cells (~1×10^6) were incubated in six-well plates overnight. On the day of the experiment, HT-29 cells were first incubated for 2 h at 37°C in the presence of 100,000 cpm of each of the ^{177}Lu-radioconjugates to reach the plateau of internalized radioactivity. Upon completion of the incubation, cells were washed five times with medium to remove the unbound peptide. Then, fresh medium was put in each well as the reservoir for efflux. At 0, 1, 2, 4 and 24 h, the medium for each time point was harvested for quantitative analysis of ligand efflux. Surface-bound radioactivity was removed by washing the cells twice with an acidic buffer (50 mM glycine-HCl/0.1 M NaCl buffer, pH 2.8). The cells were then lysed at 37°C using a 10 % aqueous SDS solution to quantify the remaining internalized fractions. The radioactivity in the effluxed, surface-bound and internalized fractions for each radioconjugate was determined using a gamma counter. The effluxed fraction is expressed as a percentage of the total amount, which is the sum of the effluxed, surface-bound and fraction remaining in the cell.

Metabolic stability in human serum and conditioned medium

The stability of ^{177}Lu-N1 in human serum and cell medium was determined. Conditioned medium refers to medium in which cells were cultured at least for one day, as medium obtained under these conditions is believed to contain proteases excreted from HT-29 cells. The conditioned medium was prepared by centrifuging at 4000 × *g* for 2 min to remove cells or cell debris. Briefly, 50 μL of HPLC-purified peptide in PBS (1.85 MBq, 50 μCi, 15 ng) was added to 50 μL human serum (MP Biomedicals, LLC (Solon, OH)) or conditioned medium and incubated at 37 °C for up to 24 h. After the incubation, 100 μL of a mixture of ethanol and acetonitrile (v/v = 1:1) was added to precipitate the serum proteins. The resulting mixture was centrifuged at 12000 × *g* for 10 min. The supernatant was collected and purged with N_2 gas for 20 min to remove the ethanol and acetonitrile. The resulting sample was dissolved in 100 μL water and injected into RP-HPLC for analysis using the gradient described above.

In vivo biodistribution studies

Biodistribution studies were carried out using HT-29 tumor bearing SCID mice. Each mouse (average weight, 20 g) received an intravenous bolus, via the tail vein, of the radio-RP-HPLC purified ^{177}Lu-N1 (280 kBq, 7.5 μCi, 2.25 ng) in 100 μL of saline. Four-hour post injection, the mice were sacrificed and the amount of radioactivity in the tumors and other tissues (blood, heart, lung, stomach, pancreas, spleen, liver, kidney, small intestine and

colon) were counted by gamma counter. The excised tissues were weighed and results were expressed as percentage of injected dose per gram of tissue (%ID/g). Biodistribution radiation was measured with a NaI (Tl) well detector from AlphaSpectra, Inc. (U.S.). Blocking studies were carried out by co-injection with excess unlabeled N1 (250 μg).

SPECT/CT imaging with ^{177}Lu-N1

For SPECT/CT imaging studies, HT-29 tumor xenograft mice were injected i.v. with ^{177}Lu-N1 (37 MBq, 1 mci, 300 ng) in 100 μL of saline and sacrificed for scanning 2 h post-injection. Images were acquired for 1 h using a FLEX Triumph single photon emission computed tomography system/X-ray computed tomography (SPECT/CT) and software (Gamma Medica, Inc., Northridge, CA).

Statistical analysis

Comparisons of each two groups for IC_{50}, internalization and efflux studies, were analyzed by the unpaired two-tailed Student's t test, and *P* values of less than 0.05 were considered statistically significant.

RESULTS

Synthesis and radiolabeling

Four NT analogs were synthesized by SPPS using the DOTA-**X**-[N-α-Me^{8},Dmt^{11},Tle^{12}]NT(6–13) paradigm depicted in Figure 1, where **X** represents a series of hydrocarbon linkers of increasing length. Initial attempts at the synthesis of the peptides by SPPS gave unacceptably poor yields. Evaluation of the crude material by LC-MS revealed that a significant portion was composed of terminated peptide chains and deletion peptides that originated at or after, respectfully, the N-methyl arginine. With the premise that the sterics of the secondary amine were negatively affecting coupling yields, we made the following modifications to our SPPS protocol: 1) for all coupling reaction, the concentration of the coupling agent, COMU, was increased 4-fold, from 0.125 M to 0.5 M; 2) the time allowed for Fmoc-deprotection of all amino acids was increased 2-fold, from 3 min to 6 min; and 3) for the two amino acids directly following the N-methyl arginine, the coupling time was increased from 5 min to 10 min and the reaction temperature was increased from 75 °C to 95 °C. With these modifications, the isolated yields of conjugates N0–3, after RP-HPLC purification, were substantially improved from less than 1% to greater than 10%. The purified conjugates were subsequently labeled with $^{177/nat}LuCl_3$ ($t_{½}$ = 6.75 days for $^{177}LuCl_3$) by co-incubation in an ammonium acetate buffer (pH = 5.5) for 60 min at 90 °C. The radiochemical yields for ^{177}Lu-N0, ^{177}Lu-N1, ^{177}Lu-N2 and ^{177}Lu-N3 were 91%, 94 %, 98% and 95%, respectively. RP-HPLC retention time, mass spectrometric identification and yields of the unlabeled conjugates and ^{nat}Lu-conjugates are listed in Table 1.

Distribution coefficient

To evaluate the impact of the hydrocarbon linkers on water solubility of the radioconjugates, the octanol-PBS distribution coefficients at pH 7.4 were measured. The log $D_{oct/water}$ values

for ^{177}Lu-N0, ^{177}Lu-N1, ^{177}Lu-N2 and ^{177}Lu-N3 were −3.45 ± 0.05, −3.15 ± 0.05, −3.11 ± 0.05 and −2.99 ± 0.03, respectively.

Receptor saturation

To establish the surface expression of the NTR1 on the HT-29 cell line, receptor saturation studies were performed using $^{177/nat}$Lu-N1. $^{177/nat}$Lu-N1 bound well to the surface of HT-29 cells, and this binding could be blocked with the addition of unlabeled NT, thus implying the specific blockage of NTR1. From these studies, carried out at 4 °C to prevent receptor-mediated endocytosis, the NTR1 expression was found to be 85000 ± 1000 binding sites per HT-29 cell with a dissociation constant (K_d) of 42 ± 8 nM. The receptor saturation curve has been shown in **Supporting information, Figure 1**.

In vitro competitive binding studies

The NTR1 binding affinity of the unlabeled conjugates and ^{nat}Lu-conjugates was investigated by competitive binding studies using HT-29 cells. Both unlabeled conjugates and ^{nat}Lu-conjugates demonstrated nanomolar binding affinities. The IC_{50} values for unlabeled N1, N2 and N3 were in the same range as full NT peptide. In contrast, the IC_{50} value for unlabeled N0 was higher than that of NT ($P < 0.01$), indicating lower binding affinity to the NTR1. A similar trend was observed for the ^{nat}Lu-labeled conjugates. ^{nat}Lu-N0 had the lowest affinity for the NTR1 relative to ^{nat}Lu-N1, ^{nat}Lu-N2 and ^{nat}Lu-N3 ($P < 0.01$) (Table 1).

In vitro internalization and efflux studies

The effect of the linker modifications on the rates of internalization (Figure 2) and efflux (Figure 3) of the radioconjugates was investigated in HT-29 cells. The cellular uptake of the radioconjugates, represented as a percentage of total activity added, was evaluated at 15, 30, 60, and 120 min time points. The cellular uptake consisted of internalized and surface-bound radioactivity. For ^{177}Lu-N0, ^{177}Lu-N2 and ^{177}Lu-N3, the internalization of these radioconjugates was essentially identical over the initial 60 min time period. However, by 120 min post-incubation, a statistically significant increase was observed with overall uptake of ^{177}Lu-N0 > ^{177}Lu-N2 > ^{177}Lu-N3 (3.69% ± 0.17%, 3.14% ± 0.10%, 2.74% ± 0.02%, respectively, $P < 0.0001$). After the 15 min time point, ^{177}Lu-N1 demonstrated substantially higher levels of uptake (2.66% ± 0.02%) relative to the other radioconjugates. By the 120 min time point, ^{177}Lu-N1 had the highest level of overall uptake with 4.38% ± 0.10% of total activity added.

Efflux studies were conducted to determine if a structure-activity relationship exists with regard to the externalization of the internalized radioconjugates. The efflux of these radioconjugates was investigated at the 1, 2, 4 and 24 h time points. At 1 h post-incubation, ^{177}Lu-N2 demonstrated higher levels of effluxed radioactivity (26% ± 0.8%) relative to the other radioconjugates (18–21%). However, the percentage of externalized radioactivity was largely indistinguishable for all of the radioconjugates investigated by 2 h. At the 4 h time point, the effluxed fraction for ^{177}Lu-N1 (29% ± 0.4%) was lower than that for ^{177}Lu-N0, ^{177}Lu-N2, ^{177}Lu-N3 (33% ± 2.5%, 34% ± 0.9% and 36% ± 3.6%, respectively, $P < 0.01$). Overall, the percent of initial internalized radioactivity effluxed

from the cells ranged from 25–32 % by the 24 h time point (**Supporting information, Table 1**).

Metabolic stability

NT is known to be susceptible to serum proteases[10]. The targeting vector used in our radioconjugates contains modifications to inhibit metabolic cleavage[11]. To establish if the structural modifications, the DOTA, or the N-terminal linker altered metabolic stability, the stability of ^{177}Lu-N1 was investigated over a 24 h period in PBS (not shown), the conditioned (used) medium, and human serum. Under the conditions of the study, > 95% of the radioactivity was recovered for analysis from each sample. Evaluation of these samples by radio-RP-HPLC revealed no degradation over a 24-h time period (Figure 4).

In vivo biodistribution and microSPECT/CT imaging studies

Based on the *in vitro* studies, ^{177}Lu-N1 was deemed our best overall candidate as a balance of the affinity, internalization and efflux. Therefore, ^{177}Lu-N1 was chosen for our preliminary *in vivo* investigation. Using the HT-29 xenograft mouse model, we evaluated the *in vivo* biodistribution of ^{177}Lu-N1 at the 4 h time point, data given in Figure 5. The i.v. administered ^{177}Lu-N1 effectively cleared from the blood (0.02 ± 0.01 % ID/g) by 4 h. As expected given the hydrophilic nature of ^{177}Lu-N1, the clearance of radioactivity preceded largely through the renal system with 86.3 ± 6.0 %ID being excreted in the urine. As a result of the high renal clearance, the kidneys exhibited significant retention (17.0 ± 2.2 %ID/g) at the 4 h time point. In addition, both the small and large intestines, known to be NTR1-positive tissues, exhibited retention of 1.4 ± 0.3 and 0.6 ± 0.1 %ID/g. This retention was largely found to be NTR1-receptor mediated as it could be effectively blocked by co-injection of 250 μg of unlabeled N1. For all other non-target tissues, ^{177}Lu-N1 demonstrated good overall clearance. At the 4 h time point, ^{177}Lu-N1 displayed good *in vivo* tumor targeting and retention, with a total accumulation of 3.1 ± 0.4 %ID/g. Accumulation in the tumor was shown to be NTR1-receptor specific with 86.6 ± 4.5 % reduction in uptake upon blocking. The ratio of tumor to blood was 123 ± 10, tumor to kidney was 0.2 ± 0.02, tumor to liver was 9.3 ± 1.6, and tumor to muscle was 111 ± 10 (**Supporting information, Table 2**).

Using microSPECT/CT, we evaluated the imaging potential of ^{177}Lu-N1 at 2 h post-administration (Figure 6). Overall, the images correlated well with the biodistribution studies carried out at the 4 h time point. With the exception of the kidneys, little signal was observed in non-target tissues. The uptake of ^{177}Lu-N1 in the HT-29 tumors was clearly visible in the flanks of the mice. As expected, the kidneys, the major pathway for biological clearance, were also readily observed.

Discussion

To date, NTR1-targeted peptides have been labeled with a number of clinically relevant radiometals, such as ^{99m}Tc, ^{111}In and ^{68}Ga[11,15,21–23]. In recent years, ^{177}Lu, a theranostic radioisotope, has received increasing attention for potential clinical applications due to its dual emission characteristics[24–27]. Upon decay, ^{177}Lu emits therapeutic beta

particles (E_{avg} = 133 keV) and gamma rays (113 and 210 keV, 6% and 10%) that are suitable for SPECT diagnostic imaging. Using ^{177}Lu allows the potential for one radiopharmaceutical to be used as both a diagnostic and radiotherapeutic, thus negating the need for a "matched-pair" system (e.g., ^{111}In and ^{90}Y) for imaging and therapy. In general, the goal of any chelation system in a radiopharmaceutical design is to retain the radionuclide during its *in vivo* lifetime. The most common polyaminocaboxylate chelator utilized in NTR1-targeted agent design is diethylenetriamine pentaacetic acid (DTPA)[11,28–30]. Unfortunately, DTPA forms a complex with ^{177}Lu that in known to be unstable *in vivo* [31]. Conversely, DOTA, due to its cyclic nature and steric inhibition, is known to form *in vivo* stable ^{177}Lu complexes, as demonstrated by numerous preclinical and clinical studies[24,27,31]. At the same time, DOTA, when placed too closely to the pharmacophore, has been shown to sterically inhibit the efficacy of receptor-targeted peptides[17,32]. This has given us the impetus to investigate the impact of the ^{177}Lu-DOTA chelation-complex on the performance of a NTR1-targeted pharmacophore (i.e., [N-α-Me^{8},Dmt^{11},Tle^{12}]NT(6–13)). To that end, we synthesized and evaluated a series of these NTR1-targeted conjugates, structurally depicted in Figure 1, with hydrocarbon linkers of 0, 4 (β-Ala), 6 (5-Ava) and 9 (8-Aoc) atoms in length.

Under our standard SPPS conditions, initial attempts to synthesize the conjugates, N0–3, in good yield was unsuccessful. Analysis of the crude material revealed that the majority of the peptides formed were termination or deletion products that stem from the incorporation of the N-methyl arginine at position 8. This is not too surprising given that it is recognized that the formation of N-methylated amides can be more difficult due to increased steric interference[33]. Adjustments to more vigorous conditions (i.e., increased temperatures and longer reaction times) gave substantially better yields of the desired peptides.

Receptor saturation studies of NTR1-positive HT-29 human colon cancer cells revealed a receptor density of approximately 85,000 ± 1000 per cell and a K_d value of 42 ± 8 nM. Relative to literature, our determined K_d is higher than values reported from other groups (1.5- 15 nM), but this moderate difference in values is likely attributable to different experimental conditions (e.g., different ligands and temperature)[12,34,35]. Of particular note, our studies were performed at 4 °C to inhibit internalization; while, literature reports were carried out at 24 or 37 °C. At these elevated temperatures, the internalized activity would likely lead to an overestimate (lower value) in the disassociation constant.

Based on the competitive binding assays, ^{177}Lu-N0, as well as the unmetallated peptide (N0), exhibited binding affinities that were roughly two fold lower than the corresponding analogs with hydrocarbon linkers. While this decrease in binding affinity is relatively modest, it does show that the steric bulk of the DOTA affects the NTR1 binding efficacy of the [N-α-Me^{8},Dmt^{11},Tle^{12}]NT(6–13) pharmacophore. Inclusion of a 4 atom hydrocarbon linker (i.e., β-Ala) appears to alleviate the steric inhibition of the chelator. Extension of the hydrocarbon linker beyond 4 atoms, as is the case for N2, N3, ^{nat}Lu-N2 and ^{nat}Lu-N3, does not lead to substantial increases in binding affinities. Interestingly, linker length does seem to play a more important role in the internalization of the NTR1-targeted agents. For ^{177}Lu-N1, the β-Ala linker gives a substantially higher percentage of internalization relative to the other analogs. This is followed by ^{177}Lu-N0, ^{177}Lu-N2 and ^{177}Lu-N3. It is interesting

that ^{177}Lu-N0 out-performed ^{177}Lu-N2 and ^{177}Lu-N3 in spite of having a lower binding affinity. It appears that even with high binding affinities, radioconjugates with longer hydrocarbon linkers, ^{177}Lu-N2 and ^{177}Lu-N3, did not induce receptor-mediated internalization as well as those with short or no hydrocarbon linkers, ^{177}Lu-N1 and ^{177}Lu-N0, respectfully. Why the longer linker length would affect the ability of the pharmacophore to activate the NTR1 is not clear. Relative to internalization, linker length had little effect on efflux patterns of the radioconjugates. One noteworthy observation was the small decrease in percentage efflux from 4 to 24 h time points. This suggests that externalized radioactivity (decay normalized) is being recycled back into the cell. It seems unlikely that this is through a receptor-mediated process, but may be attributable to pinocytosis of effluxed radioactivity over time.

As previously mentioned, the [N-α-Me^{8},Dmt^{11},Tle^{12}]NT(6–13) pharmacophore contains several modifications that significantly reduce enzymatic degradation of the pharmacophore *in vitro* and *in vivo*[11]. Utilizing ^{177}Lu-N1, our best performing conjugate, the stability of this NTR1-targeted agent was evaluated in PBS, conditioned medium and human serum. No discernible degradation was observed from these conditions over a 24 h period. This is expected based on the reported *in vitro* stability data of analogs with similar modifications[11,28]. Thus, as anticipated, the DOTA and the hydrocarbon linkers did not significantly alter *in vitro* stability of the pharmacophore at least over the monitored time frame. While no *in vitro* degradation was found for the [N-α-Me^{8},Dmt^{11},Tle^{12}]NT(6–13) peptide, Gruaz-Guyon and co-workers have demonstrated that this pharmacophore does exhibit significant *in vivo* metabolism in as little as 15 min post-injection[11]. This is an important consideration, as others have pointed out, when evaluating *in vivo* data[36]. Although the stability studies were not carried out with ^{177}Lu-N0, ^{177}Lu-N2 and ^{177}Lu-N3, we assume similar stabilities given the relative similarity of the radioconjugates.

^{177}Lu-N1 was chosen for preliminary *in vivo* investigations due to its superior *in vitro* properties. At the 4 h time point, very little of the administered radioactivity remained in the blood pool. The majority of the radioactivity (85% of the ID) was cleared by the renal system which contributed to the substantial level of accumulation in the kidneys (17.0 ± 2.2 %ID/g). Significant kidney accumulation was also observed in the SPECT/CT imaging studies. Curiously, an analog (LB119) reported with the same [N-α-Me^{8},Dmt^{11},Tle^{12}]NT(6–13) pharmacophore demonstrated substantially less renal accumulation (2.4 ± 0.2 %ID/g at 3 h p.i.)[11]. The distinct differences between the two analogs may be explained by the charge of each radioconjugate. On the N-terminal portion of ^{177}Lu-N1, the peptide contains three positively charged amino acid residues (i.e. lysine and two arginines) yielding a total +2 charge for the radioconjugate. Comparatively, the N-terminus of LB119 has the same three amino acids, but the charge of the lysine amino acid has been neutralized, by conjugation, to yield a total +1 charge for the agent. For radiolabeled peptides, the effect of charge and charge distribution on kidney accumulation has been well established[37–39]. In general, radiolabeled peptides with increasing positive charges tend to exhibit higher levels of kidney accumulation. This has been attributed, at least in part, to non-specific uptake by the surface proteins megalin and cubilin[40]. The non-specific nature of ^{177}Lu-N1 uptake in the kidney was confirmed by observation that blocking studies did not reduce accumulation.

^{177}Lu-N1 demonstrated excellent tumor uptake and retention with 3.1 ± 0.4 %ID/g at the 4 h time point. In comparison to LB119, ^{177}Lu-N1 demonstrated a 2 fold higher HT-29 tumor retention at 4 h than LB119 (1.41 ± 0.05 %ID/g) at 3 h post-administration. Given the structural similarities of the pharmacophores, the significant ($p < 0.0001$) increase in tumor uptake and retention of ^{177}Lu-N1 may be attributable to the charge of the radioconjugate as observed with the kidneys. Alternatively, this dissimilarity may be due to the purity of the prepared radioconjugates. ^{177}Lu-N1 was obtained as a peak-purified product from HPLC whereas LB119 was prepared without HPLC purification. The lack of purification of LB119 likely resulted in a small amount of unlabeled conjugate being co-injected with the radioconjugate, which may negatively impact NTR1 uptake. To what extent these factors play into the higher retention of the ^{177}Lu-N1 is not clear at this time. Small animal SPECT/CT imaging studies demonstrated significant tumor accumulation at 2 h post-administration and overall agrees well with the biodistribution data obtained at the 4 h time point.

Conclusion

We investigated the steric impact of the DOTA chelator and the length of hydrocarbon spacers on the biological performance of the [N-α-Me^{8},Dmt^{11},Tle^{12}]NT(6–13) pharmacophore. In conclusion, we found that the DOTA does negatively impact the binding affinity of the studied NTR1-targeted peptide. Optimal binding affinity could be restored by incorporation of a 4-atom hydrocarbon linker. Our best candidate (^{177}Lu-N1) demonstrated substantial tumor accumulation, but the increase in renal retention relative to other literature analogs is likely due to the higher overall positive charge of the agent.

Acknowledgement

We thank Dr. Katherine Estes and the Bioimaging Core at UNMC for assistance in SPECT/CT imaging. The authors would like to gratefully acknowledge the National Institutes of Health (1 R01 CA179059 01A1) and the National Institutes of Health (5 P20 GM103480 07 5014) for the funding and support of this research.

Abbreviation

NTR1	Neurotensin receptor 1
NT	Neurotensin
IC_{50}	50% inhibition concentration
DOTA	1,4,7,10-tetraazacyclododecane-1,4,7,10-tetraacetic acid
Fmoc-5-Ava-OH	5-(Fmoc-amino) pentanoic acid
Fmoc-8-Aoc-OH	8-(Fmoc-amino) octanoic acid
DIEA	*N*,*N*-diisopropylethylamine
DMF	*N*,*N*-dimethylformamide
DCM	dichloromethane
DCC	*N*,*N*'-dicyclohexylcarbodiimide

NMP	N-methylpyrrolidone
HEPES	4-(2-hydroxyethyl)-1-piperazineethanesulfonic acid
COMU	(1-Cyano-2-ethoxy-2-oxoethylidenaminooxy)dimethylamino-morpholino-carbenium hexafluorophosphate

References

1. Vincent JP. Neurotensin receptors: binding properties, transduction pathways, and structure. Cell Mol Neurobiol. 1995; 15:501–512. [PubMed: 8719037]
2. Gui X, Guzman G, Dobner PR, Kadkol SS. Increased neurotensin receptor-1 expression during progression of colonic adenocarcinoma. Peptides. 2008; 29:1609–1615. [PubMed: 18541341]
3. Souazé F, Dupouy S, Viardot-Foucault V, Bruyneel E, Attoub S, Gespach C, et al. Expression of neurotensin and NT1 receptor in human breast cancer: a potential role in tumor progression. Cancer Res. 2006; 66:6243–6249. [PubMed: 16778199]
4. Ehlers R, Kim S, Zhang Y. Gut peptide receptor expression in human pancreatic cancers. Ann Surg. 2000; 231:838–848. [PubMed: 10816627]
5. Swift SL, Burns JE, Maitland NJ. Altered expression of neurotensin receptors is associated with the differentiation state of prostate cancer. Cancer Res. 2010; 70:347–356. [PubMed: 20048080]
6. Carraway RE, Plona AM. Involvement of neurotensin in cancer growth: evidence, mechanisms and development of diagnostic tools. Peptides. 2006; 27:2445–2460. [PubMed: 16887236]
7. Dupouy S, Viardot-Foucault V, Alifano M, Souazé F, Plu-Bureau G, Chaouat M, et al. The neurotensin receptor-1 pathway contributes to human ductal breast cancer progression. PLoS One. 2009; 4:e4223. [PubMed: 19156213]
8. Sarret P, Kitabgi P. Neurotensin and Receptors. Encycl. Neurosci. 2010:1021–1034.
9. Myers R, Shearman J, Kitching M, Ramos-Montoya A, Neal D, Ley S. Cancer, chemistry, and the cell: molecules that interact with the neurotensin receptors. ACS Chem Biol. 2009; 4:503–525. [PubMed: 19462983]
10. Kitabgi P, Nadai FDE, Rovere C, Bidard J, Antipolis UDN. Degradation of Neurotensin and Neuromedin N. Ann NY Acade Sci. 1992; 668:30–42.
11. Alshoukr F, Prignon A, Brans L, Jallane A, Mendes S, Talbot J-N, et al. Novel DOTA-neurotensin analogues for 111In scintigraphy and 68Ga PET imaging of neurotensin receptor-positive tumors. Bioconjug Chem. 2011; 22:1374–1385. [PubMed: 21662976]
12. García-Garayoa E, Bläuenstein P, Blanc A, Maes V, Tourwé D, Schubiger PA. A stable neurotensin-based radiopharmaceutical for targeted imaging and therapy of neurotensin receptor-positive tumours. Eur J Nucl Med Mol Imaging. 2009; 36:37–47. [PubMed: 18690434]
13. Bruehlmeier M, Garayoa EG, Blanc A, Holzer B, Gergely S, Tourwé D, et al. Stabilization of neurotensin analogues: Effect on peptide catabolism, biodistribution and tumor binding. Nucl Med Biol. 2002; 29:321–327. [PubMed: 11929702]
14. Alshoukr F, Prignon A, Brans L, Jallane A, Mendes S, Talbot JN, et al. Novel DOTA-neurotensin analogues for 111In scintigraphy and 68Ga PET imaging of neurotensin receptor-positive tumors. Bioconjug Chem. 2011; 22:1374–1385. [PubMed: 21662976]
15. Macs V, Garcia-Garayoa E, Bläuenstein P, Tourwé D, Maes V. Novel 99mTc-labeled neurotensin analogues with optimized biodistribution properties. J Med Chem. 2006; 49:1833–1836. [PubMed: 16509599]
16. De León-Rodríguez LM, Kovacs Z. The synthesis and chelation chemistry of DOTA-peptide conjugates. Bioconjug Chem. 2008; 19:391–402. [PubMed: 18072717]
17. Strand J, Honarvar H, Perols A, Orlova A, Selvaraju RK, Karlström AE, et al. Influence of macrocyclic chelators on the targeting properties of (68)Ga-labeled synthetic affibody molecules: comparison with (111)In-labeled counterparts. PLoS One. 2013; 8:e70028. [PubMed: 23936372]

18. Figueroa SD, Volkert WA, Hoffman TJ. Evaluation of the Pharmacokinetic Effects of Various Linking Group Using the 111In-DOTA-X-BBN(7–14)NH2 Structural Paradigm in a Prostate Cancer Model. Bioconjug Chem. 2009; 19:1803–1812. [PubMed: 18712899]
19. Lears KA, Ferdani R, Liang K, Zheleznyak A, Sherman CD, Achilefu S, et al. In Vitro and In Vivo Evaluation of 64Cu-Labeled SarAr-Bombesin Analogs in Gastrin-Releasing Peptide Receptor-Expressing prostate cancer. J Nucl Med. 2011; 52:470–477. [PubMed: 21321264]
20. Zhou Z, Wagh NK, Ogbomo SM, Shi W, Jia Y, Brusnahan SK, et al. Synthesis and in vitro and in vivo evaluation of hypoxia-enhanced 111In-bombesin conjugates for prostate cancer imaging. J Nucl Med. 2013; 54:1605–1612. [PubMed: 23896558]
21. Maina T, Nikolopoulou A, Stathopoulou E, Galanis AS, Cordopatis P, Nock Ba. [99mTc]Demotensin 5 and 6 in the NTS1-R-targeted imaging of tumours: synthesis and preclinical results. Eur J Nucl Med Mol Imaging. 2007; 34:1804–1814. [PubMed: 17594090]
22. Garayoa EG, Schweinsberg C, Maes V, Rüegg1 D, Blanc A, Bläuenstein P, Tourwé DA, Beck-Sickinger AG, Schubiger PA. New [99mTc] bombesin analogues with improved biodistribution for targeting gastrin releasing-peptide receptor-positive tumors. QJ Nucl Med Mol Imaging. 2007; 51:42–50.
23. Mascarin A, Valverde IETLM. Effect of a spacer moiety on radiometal labeled neurotensin derivatives. RadiochimActa. 2013; 101:733–737.
24. Van Vliet EI, Hermans JJ, de Ridder Ma, Teunissen JJ, Kam BL, de Krijger RR, et al. Tumor response assessment to treatment with [177Lu-DOTA0,Tyr3]octreotate in patients with gastroenteropancreatic and bronchial neuroendocrine tumors: differential response of bone versus soft-tissue lesions. J Nucl Med. 2012; 53:1359–1366. [PubMed: 22782312]
25. Kam BLR, Teunissen JJM, Krenning EP, de Herder WW, Khan S, van Vliet EI, et al. Lutetium-labelled peptides for therapy of neuroendocrine tumours. Eur J Nucl Med Mol Imaging. 2012; (39 Suppl 1):S103–S112. [PubMed: 22388631]
26. Wild D, Frischknecht M, Zhang H, Morgenstern A, Bruchertseifer F, Boisclair J, et al. Alpha- versus beta-particle radiopeptide therapy in a human prostate cancer model (213Bi-DOTA-PESIN and 213Bi-AMBA versus 177Lu-DOTA-PESIN). Cancer Res. 2011; 71:1009–1018. [PubMed: 21245097]
27. Bander NH, Milowsky MI, Nanus DM, Kostakoglu L, Vallabhajosula S, Goldsmith SJ. Phase I trial of 177lutetium-labeled J591, a monoclonal antibody to prostate-specific membrane antigen, in patients with androgen-independent prostate cancer. J Clin Oncol. 2005; 23:4591–4601. [PubMed: 15837970]
28. Alshoukr F, Rosant C, Maes V, Abdelhak J, Raguin O, Burg S, et al. Novel neurotensin analogues for radioisotope targeting to neurotensin receptor-positive tumors. Bioconjug Chem. 2009; 20:1602–1610. [PubMed: 19610615]
29. De Visser M, Janssen PJJM, Srinivasan a, Reubi JC, Waser B, Erion JL, et al. Stabilised 111In-labelled DTPA- and DOTA-conjugated neurotensin analogues for imaging and therapy of exocrine pancreatic cancer. Eur J Nucl Med Mol Imaging. 2003; 30:1134–1139. [PubMed: 12768332]
30. Zhang K, An R, Gao Z, Zhang Y, Aruva MR. Radionuclide imaging of small-cell lung cancer (SCLC) using 99mTc-labeled neurotensin peptide 8–13. Nucl Med Biol. 2006; 33:505–512. [PubMed: 16720242]
31. Li WP, Smith CJ, Cutler CS, Hoffman TJ, Ketring AR, Jurisson SS. Aminocarboxylate complexes and octreotide complexes with no carrier added 177Lu, 166Ho and 149Pm. Nucl Med Biol. 2003; 30:241–251. [PubMed: 12745015]
32. Hoffman TJ, Gali H, Smith CJ, Sieckman GL, Hayes DL, Owen NK, et al. Novel series of 111In-labeled bombesin analogs as potential radiopharmaceuticals for specific targeting of gastrin-releasing peptide receptors expressed on human prostate cancer cells. J Nucl Med. 2003; 44:823–831. [PubMed: 12732685]
33. Pattabiraman VR, Bode JW. Rethinking amide bond synthesis. Nature. 2011; 480:471–479. [PubMed: 22193101]
34. Kitabgi P, Poustis C, Granier C, Van Rietschoten J, Rivier J, Morgat JL, et al. Neurotensin binding to extraneural and neural receptors: comparison with biological activity and structure--activity relationships. Mol Pharmacol. 1980; 18:11–19. [PubMed: 6251356]

35. Mazor O, Hillairet de Boisferon M, Lombet A, Gruaz-Guyon A, Gayer B, Skrzydelsky D, et al. Europium-labeled epidermal growth factor and neurotensin: novel probes for receptor-binding studies. Anal Biochem. 2002; 301:75–81. [PubMed: 11811969]

36. Sparr C, Purkayastha N, Yoshinari T, Seebach D. Syntheses, Receptor bindings, in vitro and in vivo Stabilities and Biodistributions of DOTA-Neurotensin (8–13) Derivatives Containing β-Amino Acid Residues-A Lesson about the Importance of Animal Experiments. Chem Biodivers. 2013; 10:2101–2122. [PubMed: 24327436]

37. Garcı E, Schweinsberg C, Maes V, Brans L, Bla P, Tourwe DA, et al. Influence of the Molecular Charge on the Biodistribution of Bombesin Analogues Labeled with the [99m Tc (CO) 3] -Core. Bioconjug Chem. 2008; 19:2409–2416. [PubMed: 18998719]

38. Vegt E, de Jong M, Wetzels JFM, Masereeuw R, Melis M, Oyen WJG, et al. Renal toxicity of radiolabeled peptides and antibody fragments: mechanisms, impact on radionuclide therapy, and strategies for prevention. J Nucl Med. 2010; 51:1049–1058. [PubMed: 20554737]

39. Vegt E, Melis M, Eek A, de Visser M, Brom M, Oyen WJG, et al. Renal uptake of different radiolabelled peptides is mediated by megalin: SPECT and biodistribution studies in megalin-deficient mice. Eur J Nucl Med Mol Imaging. 2011; 38:623–632. [PubMed: 21170526]

40. Melis M, Krenning EP, Bernard BF, Barone R, Visser TJ, de Jong M. Localisation and mechanism of renal retention of radiolabelled somatostatin analogues. Eur J Nucl Med Mol Imaging. 2005; 32:1136–1143. [PubMed: 15912401]

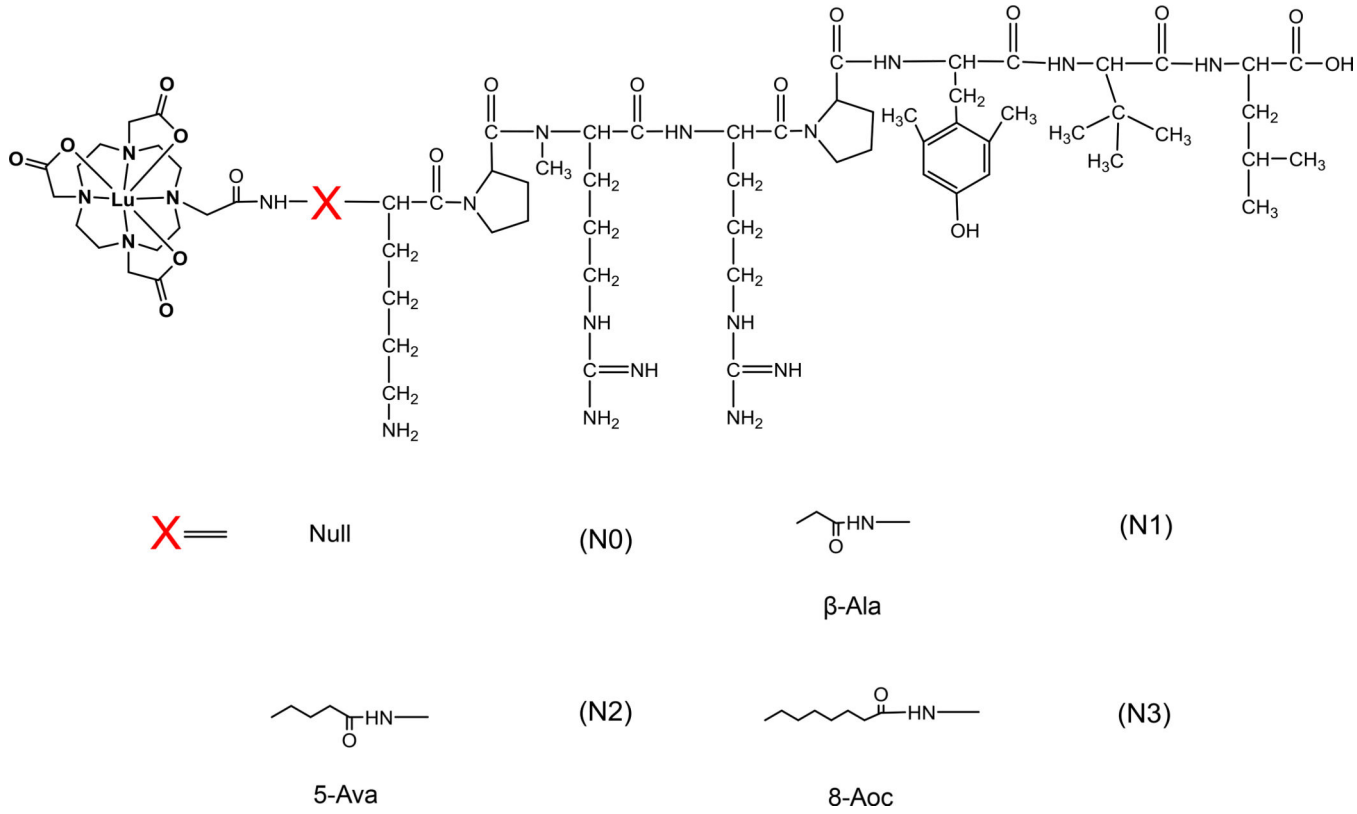

Figure 1.

Structures of the Lu-([N-α-Me^{8},Dmt^{11},Tle^{12}]NT(6–13) analogs used in this study (Lu-N0, Lu-N1, Lu-N2 and Lu-N3).

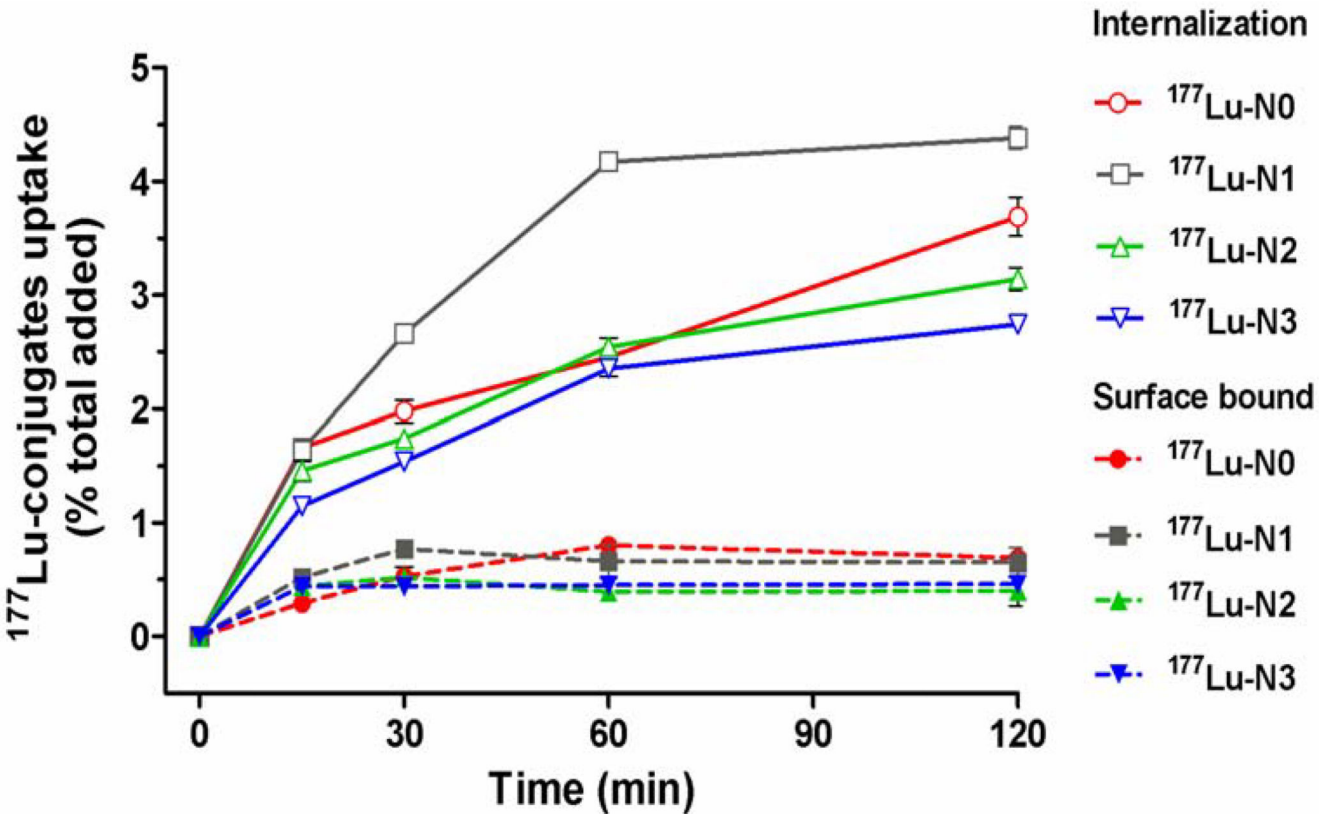

Figure 2.

Time course following the uptake of ^{177}Lu-radioconjugates, both internalization and surface bound, by HT-29 cells. Values are means ± SD (n = 6).

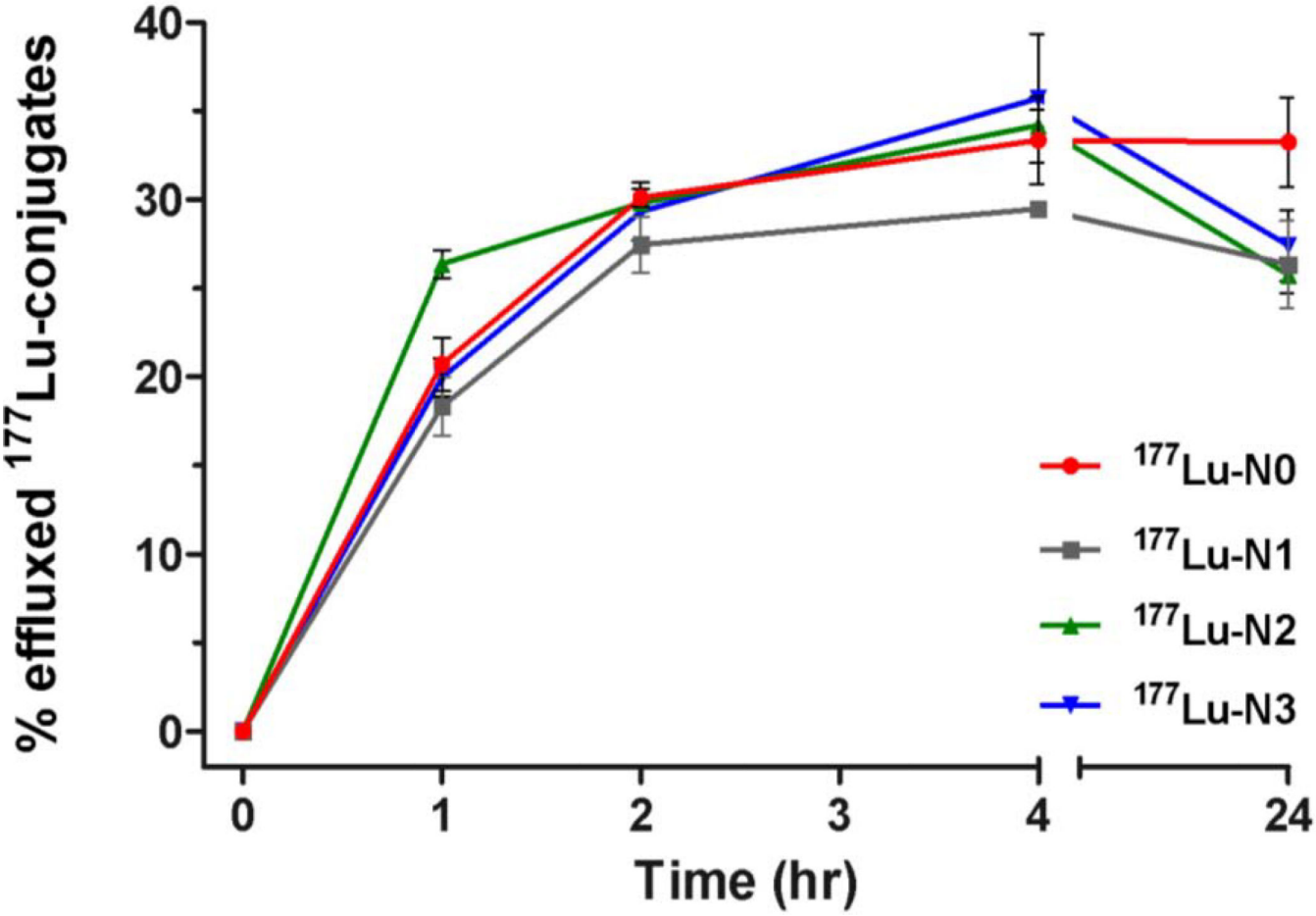

Figure 3.

Time course following the percent efflux of the internalized ^{177}Lu-radioconjugate by HT-29 cells. Values are means ± SD (n = 6).

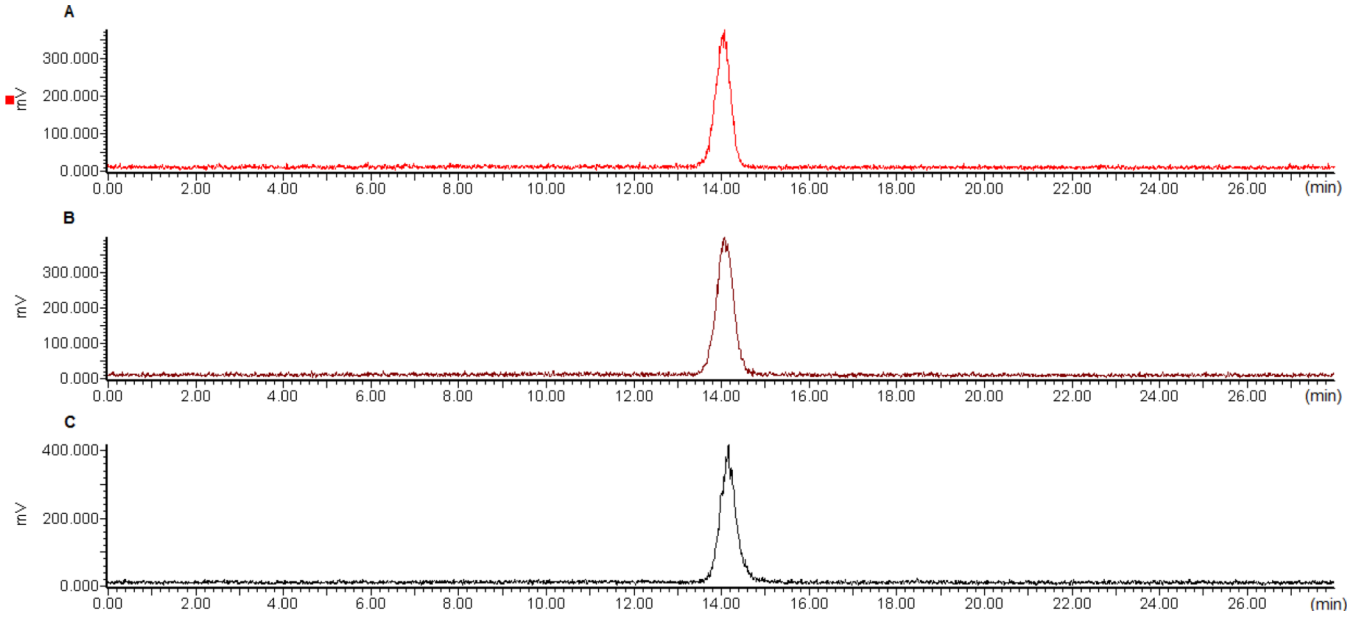

Figure 4.

Stability of ^{177}Lu-N1 in conditioned medium and human serum. Panel A: chromatograph of ^{177}Lu-N1 at start of the study, Panel B: chromatograph of ^{177}Lu-N1 after 24 h in conditioned medium, and Panel C: chromatograph of ^{177}Lu-N1 after 24 h in human serum.

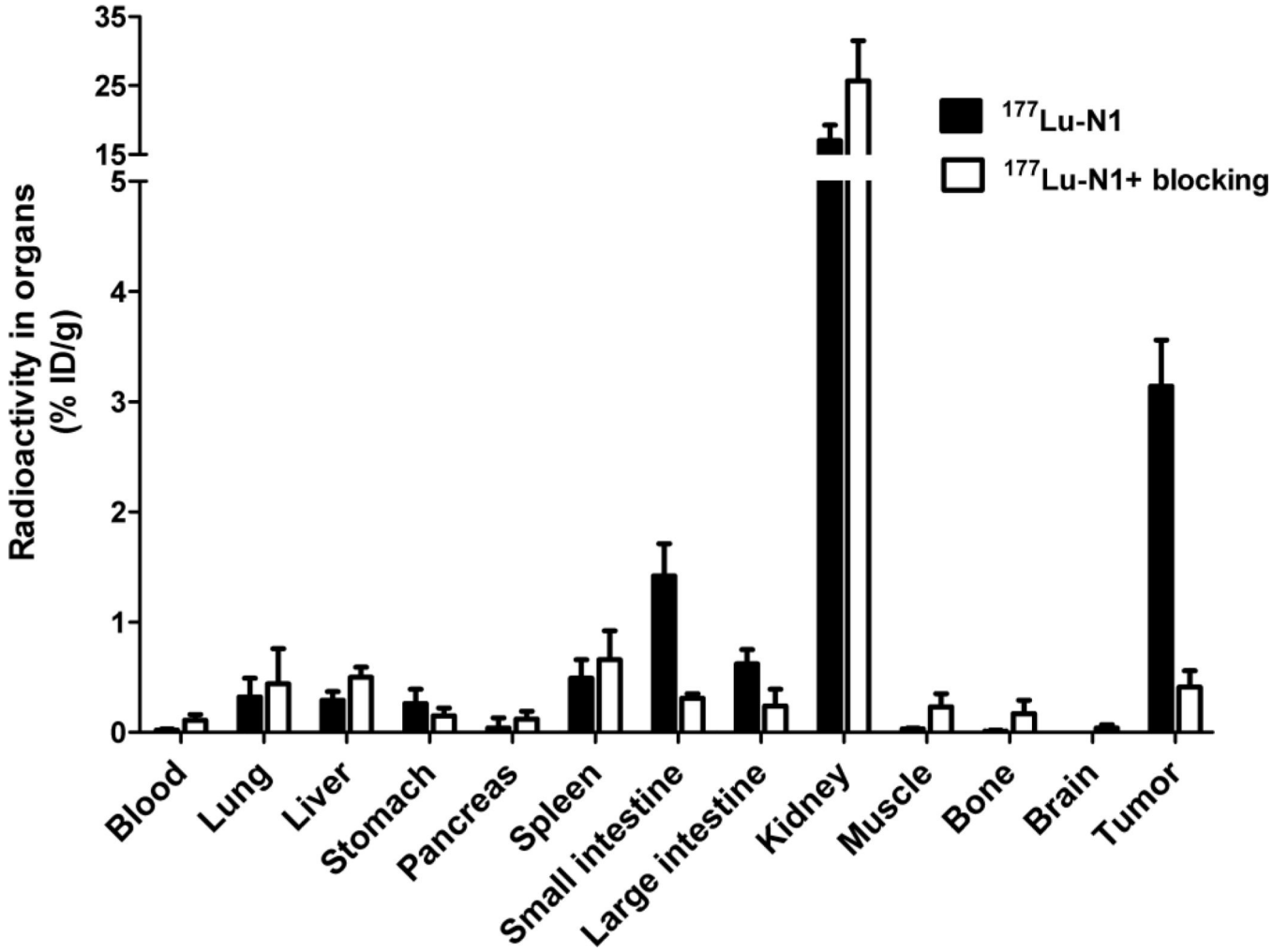

Figure 5.

Graph of the biodistribution data at 4 h p.i. for ^{177}Lu-N1 in SCID mice with HT-29 xenografts. The radioactivity accumulation is expressed as a percentage of injected dose per gram (%ID/g). Values are means ± SD (n = 5)

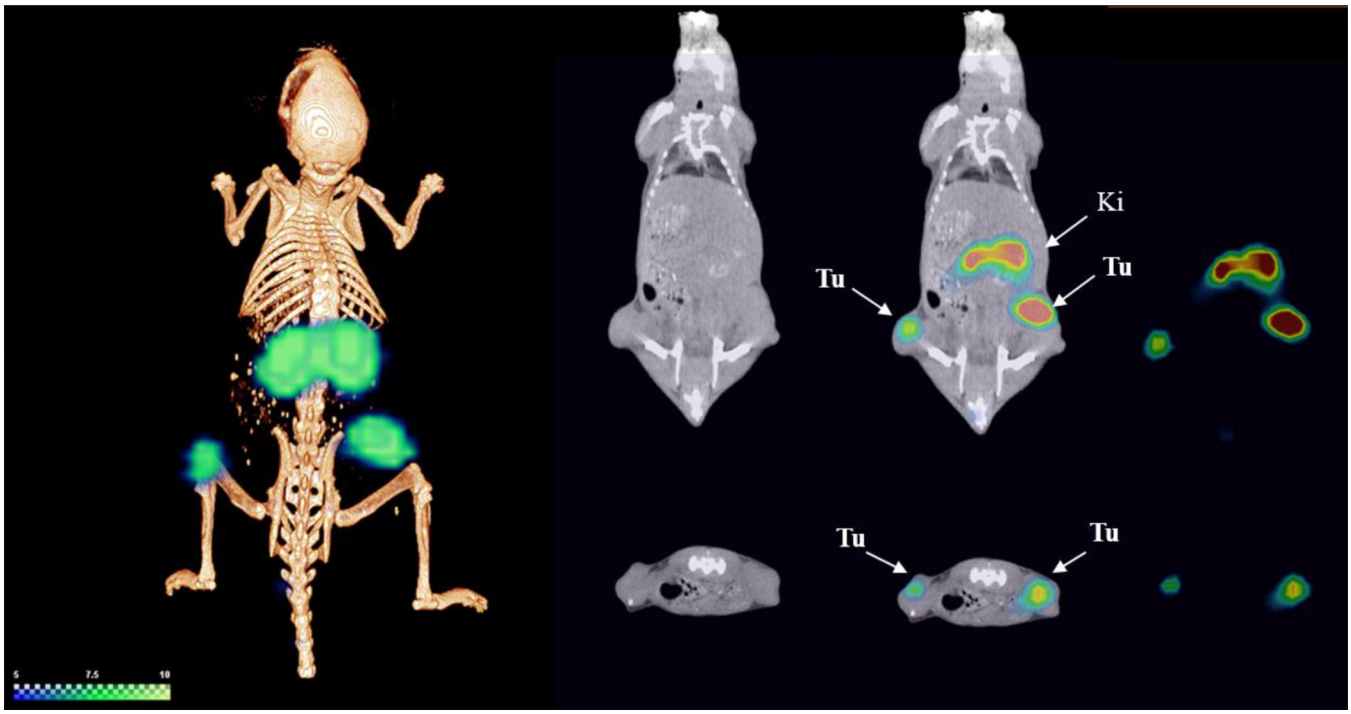

Figure 6.
SPECT/CT image of ^{177}Lu-N1 in a HT-29 xenograft mouse model at 2 h post-administration. Tu: tumor. Ki: kidney.

Table 1

Mass spectrometric and RP-HPLC characterization, yields, and IC_{50} values of NT analogs.

Analog	Sequence	MS Cal.	MS Obs. ($[M+H]^+$)	Retention Time (min)	Yields	IC_{50} ± SD (nM)
N0[a]	DOTA-Lys-Pro-(N-Me)Arg-Arg-Pro-Dmt-Tle-Leu-OH	1469.9	1470.9	13.1	10.6%	52.3 ± 1.5
N1	DOTA-β-Ala-Lys-Pro-(N-Me)Arg-Arg-Pro-Dmt-Tle-Leu-OH	1540.9	1541.9	13.9	11.1%	27.6 ± 1.3
N2	DOTA-5-Ava-Lys-Pro-(N-Me)Arg-Arg-Pro-Dmt-Tle-Leu-OH	1568.9	1569.9	10.8	10.0%	20.8 ± 1.4
N3	DOTA-8-Aoc-Lys-Pro-(N-Me)Arg-Arg-Pro-Dmt-Tle-Leu-OH	1611.0	1611.9	11.3	10.2%	21.1 ± 1.7
Lu-N0[b]	^{nat}Lu-N0[c]	1641.9	1642.8	10.6	78.1%	47.2 ± 1.2
Lu-N1	^{nat}Lu-N1	1712.9	1713.8	11.7	71.2%	27.2 ± 1.1
Lu-N2	^{nat}Lu-N2	1740.9	1741.8	10.4	72.2%	24.3 ± 1.1
Lu-N3	^{nat}Lu-N3	1783.0	1783.8	9.6	86.7%	20.3 ± 1.2
NT	—	—	—	—	—	22.3 ± 1.2

[a] For unlabeled N0-3, a Phenomenex Jupiter 10 μm Proteo 250 × 10 mm, C12 column was used with a flow rate of 5.0 mL/min

[b] For ^{nat}Lu-labeled N0-3, a Phenomenex Jupiter 10 μm Proteo 250 × 4.6 mm, C12 column was used with a flow rate 1.5 mL/min.

[c] ^{nat}Lu refers to naturally abundant lutetium isotopes.